Dynamic Performance Analysis of a Large-Scale AWS-Based Wave Power Farm Integrated Into a Single-Machine Infinite-Bus Power Grid

Quang-Son Vo
Department of Electrical Engineering
University of Science and Technology, The University of Danang
Email: vqson@dut.udn.vn

***Abstract*—This paper presents the dynamic performance analysis results of a large-scale wave power farm (WPF) integrated into a single-machine infinite-bus (SMIB) power grid. The WPF is simulated by an aggregated equivalent linear permanent magnet generator (LPMG) driven by an aggregated Archimedes wave swing (AWS)-based wave energy converter (WEC). An ultracapacitor-based energy storage system (UC-ESS) is proposed for smoothing power fluctuations generated by the studied WPF. The time-domain simulation results based on a nonlinear model of the studied system are carried out using MATLAB/SIMULINK software. The simulation results show that the output power of the AWS-based WPF fed to the power grid contains large fluctuations which can significantly degrade the dynamic stability of the studied system. The simulation results also show that the proposed UC-ESS can effectively absorb power fluctuations generated by the WPF and thus enhance the dynamic performance of the studied large-scale WPF integrated into a SMIB power grid.**

Keywords-wave power; Archimedes wave swing; ultra-capacitor; power-smoothing; time-domain simulation

I. INTRODUCTION

Nowadays, renewable energy technologies are experiencing rapid and constant implementation worldwide. In addition to wind and solar, other renewable energy sources from the oceans such as wave, tidal, and marine current are gaining more attention. Among the renewable energy sources from oceans, wave power is seen as having a huge potential for electricity generation due to its high energy density. Although the wave power technology lags far behind solar and wind, it has been increasingly researched and developed in recent years. The MW-level wave energy projects are in trial operation and demonstration phases in some countries. The modeling and control of AWS-based wave energy conversion systems have been presented in several studies [1-5]. The authors in [6] designed a SMES-battery energy storage for conditioning the outputs of WECs. The investigation of employing supercapacitors for smoothing power of WEC was reported in [7-9]. In the above-mentioned works, the dynamic characteristics of the wave energy conversion systems were studied while the impact of wave power on the main power grid was not discussed. Also, the capacity of the studied wave energy conversion systems in those papers was quite small. In this paper, the dynamic performance of a 60-MW AWS-based WPF feeding power to a SMIB power grid is investigated. A UC-ESS is proposed for absorbing power fluctuations generated by the studied WPF. The dynamic characteristics of the studied system with and without the UC-ESS are examined through time-domain simulations based on a nonlinear model of the studied system.

II. SYSTEM CONFIGURATION AND MATHEMATICAL MODELS

A. Configuration of the Studied System

Fig. 1 shows the configuration of the studied AWS-based WPF fed to a SMIB power grid. The studied WPF has a rating of 60 MW consisting of 30 wave power generation units (WPGUs). Each WPGU consists of an LPMG driven by an AWS-based WEC. The output of the LPMG is connected to the AC grid through a voltage-source converter (VSC), a DC link, a voltage-source inverter (VSI), step-up transformers, and a connection cable. For simplicity, the operating characteristics of the studied WPF are modeled as a single aggregated LPMG driven by an aggregated AWS-based WEC. The SMIB power grid includes a 125-MW synchronous generator (SG) connected to an infinite bus through a 15.5/230-kV step-up transformer and a 230-kV transmission line [10]. A UC-ESS is proposed at the DC link for smoothing power fluctuations generated by the WPF. The employed mathematical models for the subsystems shown in Fig. 1 are described hereafter.

B. Model of the AWS-Based WPF

The studied 60-MW WPF is modeled as a single aggregated LPMG driven by an aggregated AWS-based WEC. The dynamics of the AWS-based WEC can be described by [1]

$$p(z) = u_z \quad (1)$$

$$(M)p(u_z) = F_W - K_S z - K_D u_z - F_{LG} \quad (2)$$

where p is the differential operator with respect to time t ($p = d/dt$); z and u_z are the position and speed of the floater, respectively; M is the total mass of the floater and the translator of the LPMG; F_W and F_{LG} are the forces acting on the floater from the wave and from the LPMG, respectively; and K_S and K_D are the spring constant and the damping coefficient of the AWS, respectively.

The dynamic model of the LPMG based on a *dq*-reference frame fixed in the translator can be given by [1], [11]

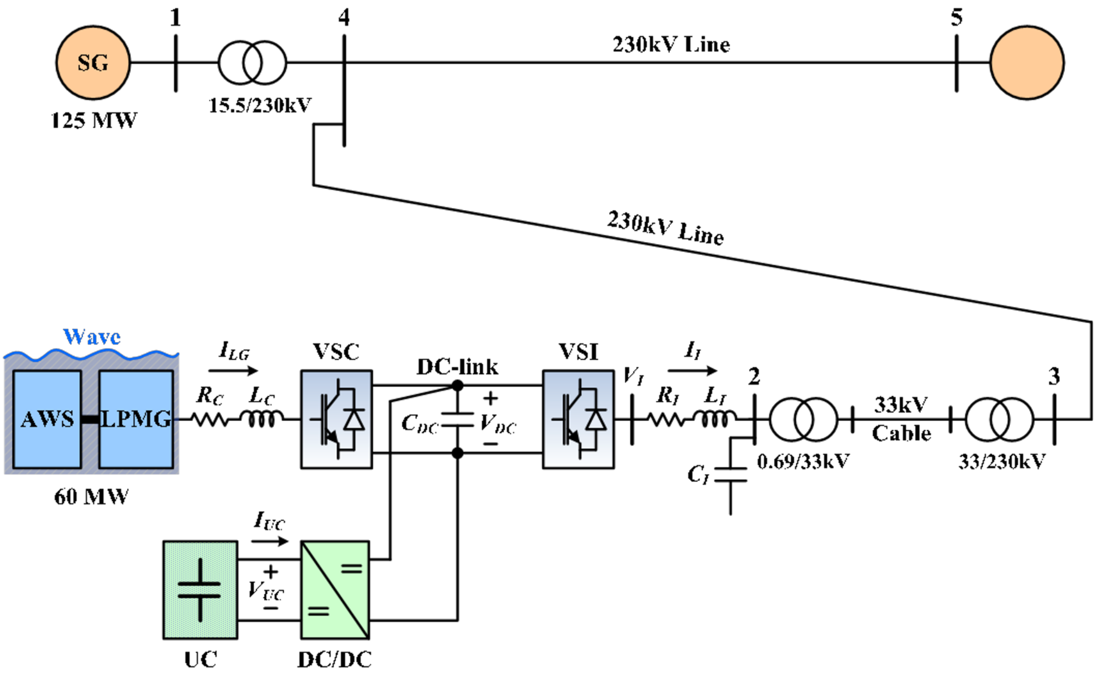

Figure 1. Configuration of the studied AWS-based WPF integrated into a SMIB power grid.

$$L_{dLG}\,p(i_{dLG}) = \omega_z L_{qLG} i_{qLG} - R_{LG} i_{dLG} - v_{dLG} \tag{3}$$

$$L_{qLG}\,p(i_{qLG}) = \omega_z \psi_{PM} - \omega_z L_{dLG} i_{dLG} - R_{LG} i_{qLG} - v_{qLG} \tag{4}$$

where i_{dLG}, i_{qLG} are the *d*- and *q*-axis currents, respectively; R_{LG} is the stator-winding resistance; L_{dLG} and L_{qLG} are the *d*- and *q*-axis synchronous inductances of the LPMG, respectively; ψ_{PM} is the flux linkage of the permanent magnet; v_{dLG}, v_{qLG} are the *d*- and *q*-axis voltages, respectively; and $\omega_z = \pi u_z/\tau_p$ (τ_p is the pole pitch of the LPMG).

C. Model of the UC-ESS

The configuration of the UC-ESS consists of the UC and the bidirectional DC/DC converter. The dynamic equations of the UC can be written as [11]

$$(C_{UC})\,p(V_{C\_UC}) = -i_{UC} - V_{C\_UC}/R_{pUC} \tag{5}$$

$$V_{UC} = V_{C\_UC} - R_{sUC} i_{UC} \tag{6}$$

where V_{UC} and I_{UC} are the voltage and current of the UC, respectively; C_{UC} is the capacitance of the UC; R_{sUC} and R_{pUC} are the series and parallel resistances representing the Joule loss and self-discharge phenomenon of the UC, respectively; and V_{C_UC} is the voltage across C_{UC}.

The bidirectional DC/DC converter is employed for interfacing the UC to the DC link. This converter can operate in Buck mode when charging the UC or in Boost mode when discharging energy into the DC link. The more detailed configuration and equivalent circuits of the bidirectional DC/DC converter can be referred to [11] while its dynamics in Buck mode and Boost mode can be described by

Buck mode:

$$(L_S)\,p(i_{UC}) = -R_S i_{UC} + V_{UC} - D_S V_{DC} \tag{7}$$

$$i_{UC\_DC} = D_S i_{UC} \tag{8}$$

Boost mode:

$$(L_S)\,p(i_{UC}) = -R_S i_{UC} + V_{UC} - (1 - D_S)V_{DC} \tag{9}$$

$$i_{UC\_DC} = (1 - D_S)i_{UC} \tag{10}$$

where L_S and R_S are the inductance and parasite resistance of the energy-storage inductor, respectively; i_{UC_DC} is the current at the DC-link side; and D_S is the duty ratio of the bidirectional DC/DC converter.

D. Model of the SG

As mentioned earlier, the studied SMIB power grid includes an SG connected to an infinite bus through a step-up transformer and a transmission line. The studied SG is modeled by employing the two-axis model of an SG. The per-unit (pu) differential equations for the two-axis model of an SG can be found in [10].

III. Control Schemes

A. Control of the VSC

Fig. 2 depicts the control block diagram of the VSC of the WPF. The objectives of this controller are to enable the WPF to convert maximum power from the waves and to minimize the power loss in the LPMG. These objectives can be achieved by controlling the *d*- and *q*-axis currents of the LPMG (i_{dLG} and i_{qLG}) [1]. The power loss in the LPMG can be minimized by setting the reference value of the *d*-axis current equal to zero, i.e. $i_{dLG\_ref} = 0$. In order for the WPF to convert maximum power from the wave, the reference value of the *q*-axis current is determined by [1]

$$i_{qLG\_ref} = \frac{2\tau_p K_D u_z}{3\pi\psi_{PM}} \quad (11)$$

B. Control of the VSI

Fig. 3 shows the control block diagram of the VSI. In order for the VSI to effectively transfer all the generated power of the WPF to the power grid, the controller of the VSI is used to maintain the DC-link voltage constant and control the voltage magnitude of Bus 2 (point of common coupling) at its reference value. The DC-link voltage and the voltage of Bus 2 are controlled via the *d*- and *q*-axis currents of the VSI (i_{dI} and i_{qI}), respectively.

C. Control of the Bidirectional DC/DC Converter

Fig. 4 illustrates the control block diagram of the bidirectional DC/DC converter of the proposed UC-ESS. This controller regulates the power charged or discharged by the UC to smooth out the power fluctuations generated by the WPF. The reference value of the power charged or discharged by the UC (P_{UC_ref}) can be determined by an averaging mechanism as shown in Fig. 5. The output power of the LPMG is first passed through a low-pass filter for averaging. The average power is then subtracted by the original power for extracting the power fluctuations which are assigned as the reference value P_{UC_ref}.

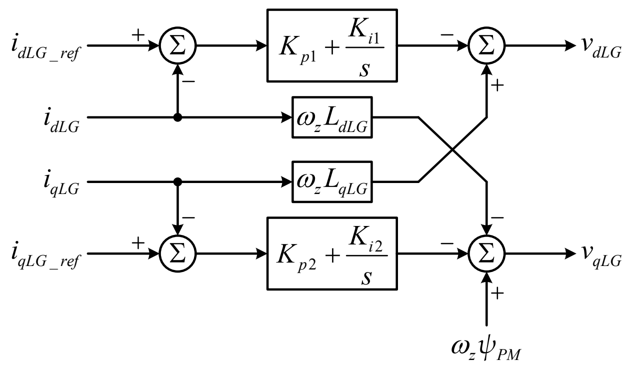

Figure 2. Control block diagram of the VSC.

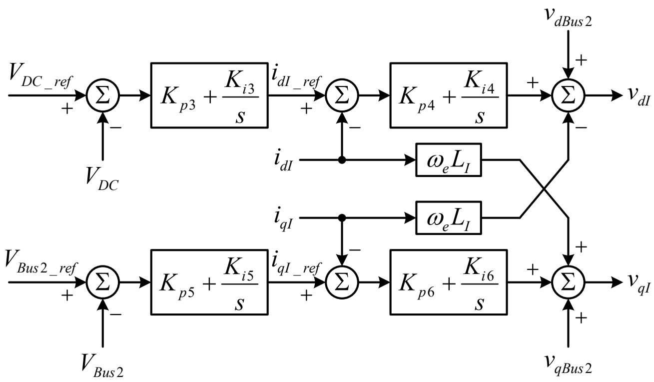

Figure 3. Control block diagram of the VSI.

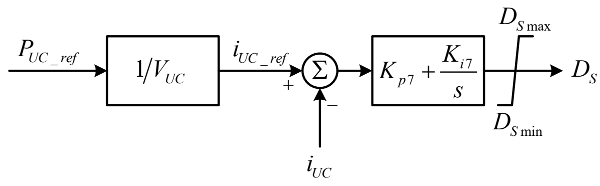

Figure 4. Control block diagram of the bidirectional DC/DC converter of the UC-ESS.

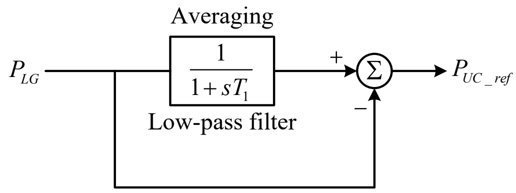

Figure 5. Determination of the reference value of the power charged or discharged by the UC.

IV. TIME-DOMAIN SIMULATION

This section employs the nonlinear-system model developed in Section 2 to examine the dynamic responses of the studied system. The employed parameters for simulation are shown in Table I. The studied system is simulated under the variations of the wave force acting on the AWS of the WPF as illustrated in Fig. 6(a). Initially, the peak amplitude and the period of the wave force are 0.9 MN and 12 s, respectively. The peak amplitude of the wave force thereafter drops to 0.45 MN at $t = 50$ s and rises to 0.8 MN at $t = 100$ s.

TABLE I. EMPLOYED PARAMETERS OF THE STUDIED SYSTEM

2-MW AWS-based WPGU
1) AWS: $K_D = 12.55\times10^6$ Ns/m, $K_S = 7.0\times10^6$ N/m, $M = 7.5\times10^3$ kg 2) LPMG: $R_{LG} = 2.2\times10^{-3}\ \Omega$, $L_{dLG} = 3.87$ mH, $L_{qLG} = 2.43$ mH, $\psi_{PM} = 23$ Wb, $\tau_p = 0.05$ m
DC link and AC sides of VSC and VSI
1) DC link: $V_{DC} = 1200$ V, $C_{DC} = 0.12$ F 2) AC side of VSC: $R_C = 0.002\ \Omega$, $L_C = 50\ \mu$H 3) AC side of VSI: $R_I = 0.002\ \Omega$, $L_I = 50\ \mu$H
UC and bidirectional DC/DC converter
1) UC for each 2-MW AWS-based WPGU: Power rating: 1MW, energy rating: 1.91MWh, $C_{UC} = 1200$ F, $R_{sUC} = 0.3\times10^{-3}\ \Omega$, $R_{pUC} = 0.52\times10^3\ \Omega$ 2) Bidirectional DC/DC converter: $R_S = 0.001\ \Omega$, $L_S = 0.005$ H
Controllers
$K_{p1} = 10$, $K_{i1} = 8\,s^{-1}$, $K_{p2} = 5$, $K_{i2} = 8\,s^{-1}$, $K_{p3} = 2.4$, $K_{i3} = 325.8\,s^{-1}$, $K_{p4} = K_{p6} = 0.4$, $K_{i4} = K_{i6} = 15\,s^{-1}$, $K_{p5} = 0.006$, $K_{i5} = 50.2\,s^{-1}$, $K_{p7} = 1.2$, $K_{i7} = 0.001\,s^{-1}$, $T_1 = 12$ s

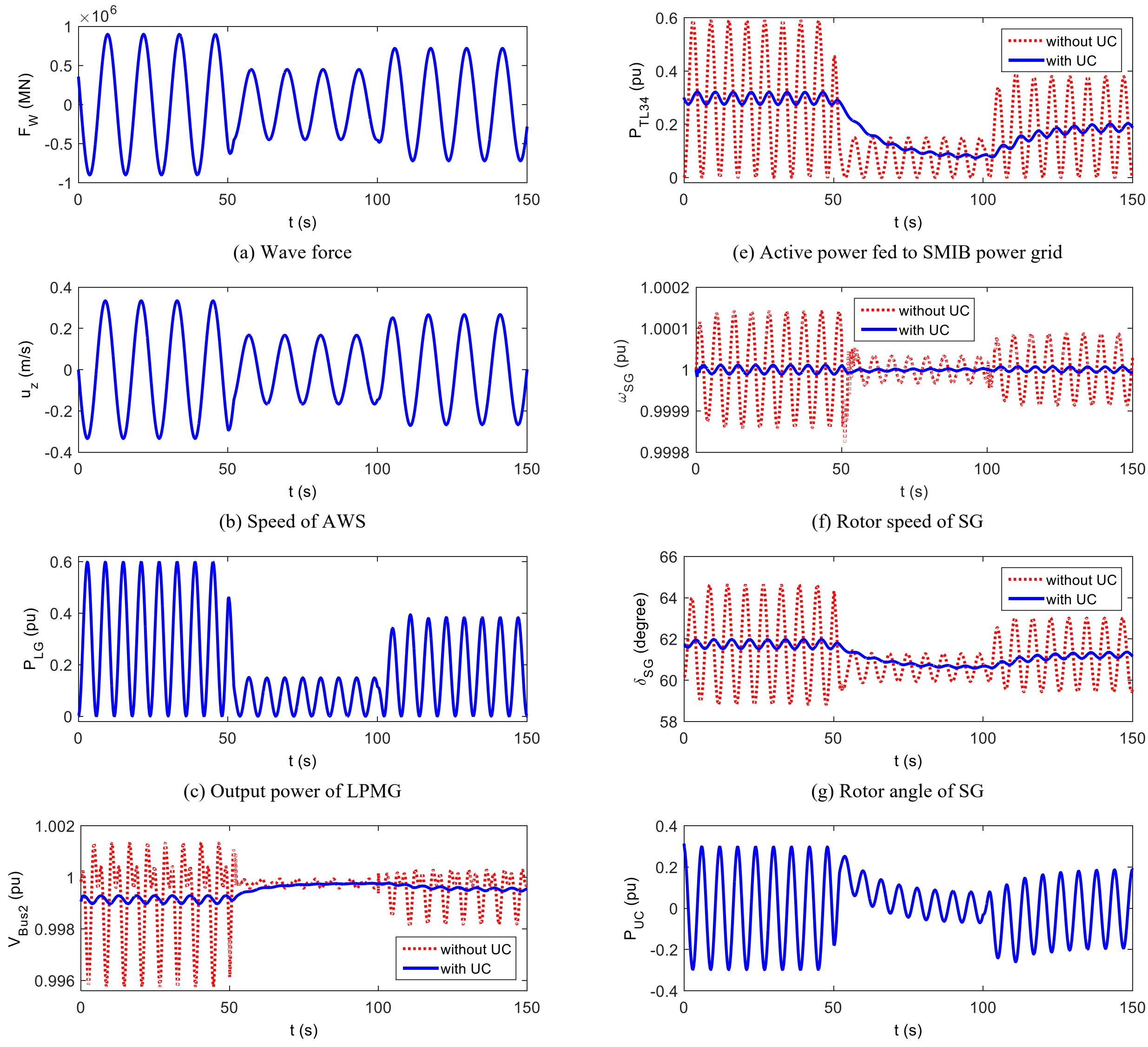

(a) Wave force (e) Active power fed to SMIB power grid

(b) Speed of AWS (f) Rotor speed of SG

(c) Output power of LPMG (g) Rotor angle of SG

(d) Voltage at Bus 2 (h) Power of UC-ESS

Figure 6. Dynamic responses of the studied system under the variations of wave force acting on the AWS.

Fig. 6(b)-(g) show the dynamic responses of the studied system under the variations of wave force. In these figures, the voltage and power are expressed in pu in a common base of 100 MVA, 230 kV, and 60 Hz.

The speed of the AWS and instantaneous output power of the LPMG of the WPF, as depicted in Fig. 6(b), (c), are continuously varied with time due to the variations of the wave force. The output power of the LPMG, as seen in Fig. 6(c), consists of the large power fluctuations. The output power of the LPMG is also significantly reduced when the peak amplitude of the wave force drops to 0.45 MN at $t = 50$ s and it is considerably increased when the peak amplitude of the wave force rises to 0.8 MN at $t = 100$ s.

Fig. 6(d)-(g) illustrate the comparative responses of some other quantities of the studied system with and without the UC-ESS such as the voltage at Bus 2, the active power fed to the SMIB power grid through the transmission line between Bus 3 and Bus 4, the rotor speed and rotor angle of the SG. It can be clearly observed from these responses that when the studied system is without the UC-ESS, the power fluctuations injected by the WPF can cause negative impacts on the dynamics of the studied SMIB power grid. On the other hand, when the studied system is equipped with the UC-ESS, the power fluctuations due to the variations of the wave can be effectively suppressed from transferring to the power grid. The power fluctuations have been compensated by the UC as illustrated in Fig. 6(h). It can be concluded from the simulation results that the UC-ESS can effectively improve the performance of the studied system under the variations of the wave force acting on the AWS of the WPF.Conclusions

This paper has presented the dynamic performance analysis results of a 60-MW AWS-based WPF integrated into a SMIB power grid. A UC-based ESS has been proposed for smoothing the power generated by the WPF fed to the SMIB power grid. The time-domain simulation results of the studied system have been examined. It can be concluded from the simulation results that large power fluctuations from the AWS-based WPF can degrade the performance of the studied system significantly. It can also be concluded that the proposed UC-based ESS can effectively absorb the power fluctuations from the WPF and hence can enhance the dynamic performance of the studied SMIB power grid connected with the AWS-based WPF.

References

[1] F. Wu, X.-P. Zhang, P. Ju, and M. J. H. Sterling, "Modeling and control of AWS-based wave energy conversion system integrated into power grid," *IEEE Trans. Power Systems*, vol. 23, no. 3, pp. 1196-1204, Aug. 2008.

[2] F. Wu, X.-P. Zhang, P. Ju, and M. J. H. Sterling, "Optimal control for AWS-based wave energy conversion system," *IEEE Trans. Power Systems*, vol. 24, no. 4, pp. 1747-1755, Nov. 2009.

[3] B. Das and B. C. Pal, "Voltage control performance of AWS connected for grid coonection," *IEEE Trans. Energy Conversion*, vol. 21, no. 2, pp. 353-361, Jun. 2006.

[4] M. I. Marei, M. Mokhtar, and A. A El-Sattar, "MPPT strategy based on speed control for AWS-based wave energy conversion system," *Renewable Energy*, vol. 83, pp. 305-317, Nov. 2015.

[5] M. Al-Dhaifallah *et al.*, "Dynamic performance enhancement of nonlinear AWS wave energy systems based on optimal super-twisting control strategy," *Ain Shams Engineering Jour.*, vol. 15, no. 5, pp. 1-20, Mar. 2024.

[6] Z. Nie, X. Xiao, Q. Kang, R. Aggarwal, H. Zhang, and W. Yuan "SMES-battery energy storage system for conditioning outputs from direct drive linear wave energy converters," *IEEE Trans. Applied Superconductivity*, vol. 23 no. 3, Jun. 2013.

[7] D. B. Murray, J. G. Hayes, D. L. O'Sullivan, and G. Egan, "Supercapacitor testing for power smoothing in a variable speed offshore wave energy converter," *IEEE Jour. Oceanic Engineering*, vol. 37, no. 2, pp. 301-308, Apr. 2012.

[8] P. Moreno-Torres, M. Blanco, G. Navarro, and M. Lafoz, "Power smoothing system for wave energy converters by means of a supercapacitor-based energy storage system," in *Proc. 2015 17th European Conf. Power Electronics and Applications*, 2015, pp. 1-9.

[9] A. Y. Elamin and A. Wahyudie, "Optimal control of a supercapacitor energy storage system for smoothing wave output power," in *Proc. 2022 Int. Conf. Electrical and Computing Technologies and Applications Electronics and Applications*, 2022, pp. 186-189.

[10] P. Kundur, *Power System Stability and Control*. New York: McGraw-Hill, 1994.

[11] L. Wang, Q.-S. Vo, and A. V. Prokhorov, "Dynamic stability analysis of a hybrid wave and photovoltaic power generation system integrated into a distribution power grid," *IEEE Trans. Sustainable Energy*, vol. 8, no. 1, pp. 404-413, Jan. 2017.